7-20-1996

Far-Field Scattering of an Axisymmetric Laser Beam of Arbitrary Profile by an On-Axis Spherical Particle

James A. Lock
Cleveland State University, j.lock@csuohio.edu

Joseph T. Hodges

Original Citation

Lock, James A. and Joseph T. Hodges. "Far-Field Scattering of an Axisymmetric Laser Beam of Arbitrary Profile by an On-Axis Spherical Particle." *Applied Optics* 35 (1996): 4283-4290.

Far-field scattering of an axisymmetric laser beam of arbitrary profile by an on-axis spherical particle

James A. Lock and Joseph T. Hodges

Experimental laser beam profiles often deviate somewhat from the ideal Gaussian shape of the TEM_{00} laser mode. In order to take these deviations into account when calculating light scattering, we propose a method for approximating the beam shape coefficients in the partial wave expansion of an experimental laser beam. We then compute scattering by a single dielectric spherical particle placed on the beam's axis using this method and compare our results to laboratory data. Our model calculations fit the laboratory data well. © 1996 Optical Society of America

1. Introduction

In recent years two different approaches have been developed for calculating scattering of a localized laser beam by a spherical particle whose diameter is comparable to the beam width. One method relies on expanding the beam in an angular spectrum of plane waves.[1,2] In the other method, the beam is expanded in terms of partial waves.[3–5] In the second approach, much has been learned about scattering of a focused beam having a Gaussian profile at its focal waist. For a number of reasons, however, the intensity profile of actual laser beams often deviates somewhat from an ideal Gaussian shape. Thus the light-scattering signature of an actual beam also deviates from the predictions of Gaussian beam scattering theory.[6] Our purpose is to perform an approximate partial wave analysis of an experimental laser beam profile and then use this partial wave analysis to compute scattering of the beam by a spherical particle placed on the beam's axis. The subject of scattering by a spherical particle placed off the beam's axis entails a number of additional considerations and thus will be treated in a separate paper.

Although the partial wave coefficients of a laser beam are related to both the magnitude and phase of the beam's electric field, measurement of the beam's intensity allows one to infer only the electric field magnitude, leaving the phase undetermined. In the Fraunhofer zone or far zone of the beam, however, the phase of the beam may be modeled. The combination of the far-zone intensity measurement and our phase modeling provides enough information to determine approximately the magnitude and phase of the coefficients in the beam's partial wave expansion.

The body of this paper is organized as follows. In Section 2 we briefly review the equations for scattering of an on-axis laser beam with an arbitrary profile by a spherical particle. In Section 3 we describe our method for approximately determining the partial wave coefficients of the beam. As a check of our method, we show that, when it is applied to a beam with a Gaussian profile, the partial wave coefficients obtained are nearly identical to the localized model Gaussian beam shape coefficients.[7,8] Finally in Section 4 we compare the predictions of our method with experimental scattering data for three different positions of a dielectric spherical particle on the beam axis. We find an excellent correspondence between our model and the experimental data in two of the three cases. We also conjecture why our results for the third case deviate somewhat from the experimental results.

2. Scattering of an On-Axis Beam by a Spherical Particle

Consider an axially symmetric monochromatic beam of electromagnetic radiation having wavelength λ and wave number

$$k = 2\pi/\lambda, \tag{1}$$

traveling along the z axis of a laboratory coordinate system whose origin is at the center of a spherical particle of radius a and refractive index n. Such a

J. A. Lock is with the Department of Physics, Cleveland State University, Cleveland, Ohio 44115. J. T. Hodges is with the Chemical Science and Technology Laboratory, National Institute of Standards and Technology, Gaithersburg, Maryland 20899.

Received 3 July 1995; revised manuscript received 11 December 1995.

0003-6935/96/214283-08$10.00/0

beam is called an on-axis beam with respect to the particle because it strikes the particle head on. If the beam were traveling parallel to the z axis rather than along it, it would strike the particle off center and thus be called an off-axis beam. The time dependence of the beam is taken to be $\exp(-i\omega t)$. The beam is assumed to be focused by a lens, and the center of the beam focal waist is at the coordinate $(0, 0, z_0)$ with respect to the particle as is shown in Fig. 1. The electric field of the beam at the focal waist is assumed to be polarized in the x direction.

Since the beam fields are derivable from a radiation potential that satisfies the Helmholtz equation,[9] the electric and magnetic fields of an on-axis beam have the following partial wave expansion with respect to the origin of coordinates at the particle center[10]:

$$\begin{aligned}
&\mathbf{E}_{\text{beam}}(r, \theta, \phi) \\
&= \frac{-iE_0 \sin\theta \cos\phi}{k^2 r^2} \hat{u}_r \sum_{l=1}^{\infty} (2l+1) i^l g_l \mathscr{J}_l(kr) \pi_l(\theta) \\
&\quad + \frac{E_0 \cos\phi}{kr} \hat{u}_\theta \sum_{l=1}^{\infty} i^l \frac{(2l+1)}{l(l+1)} g_l \\
&\quad \times [\, \mathscr{J}_l(kr) \pi_l(\theta) - i\, \mathscr{J}_l'(kr) \tau_l(\theta)] \\
&\quad - \frac{E_0 \sin\phi}{kr} \hat{u}_\phi \sum_{l=1}^{\infty} i^l \frac{(2l+1)}{l(l+1)} g_l \\
&\quad \times [\, \mathscr{J}_l(kr) \tau_l(\theta) - i\, \mathscr{J}_l'(kr) \pi_l(\theta)], \\
&\mathbf{B}_{\text{beam}}(r, \theta, \phi) \\
&= \frac{-iE_0 \sin\theta \sin\phi}{k^2 r^2} \hat{u}_r \sum_{l=1}^{\infty} i^l (2l+1) g_l \mathscr{J}_l(kr) \pi_l(\theta) \\
&\quad + \frac{E_0 \sin\phi}{kr} \hat{u}_\theta \sum_{l=1}^{\infty} i^l \frac{(2l+1)}{l(l+1)} g_l \\
&\quad \times [\, \mathscr{J}_l(kr) \pi_l(\theta) - i\, \mathscr{J}_l'(kr) \tau_l(\theta)] \\
&\quad + \frac{E_0 \cos\phi}{kr} \hat{u}_\phi \sum_{l=1}^{\infty} i_l \frac{(2l+1)}{l(l+1)} g_l \\
&\quad \times [\, \mathscr{J}_l(kr) \tau_l(\theta) - i\, \mathscr{J}_l'(kr) \pi_l(\theta)]. \qquad (2)
\end{aligned}$$

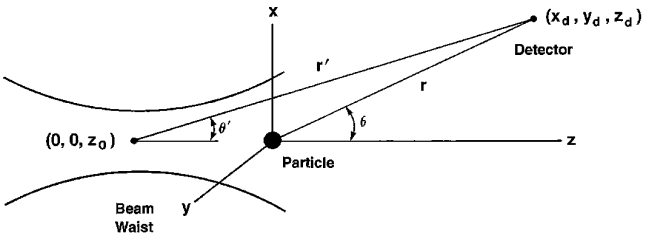

Fig. 1. Focused laser beam incident on a spherical particle whose center is at the origin of coordinates. The center of the beam focal waist is at $(0, 0, z_0)$ with respect to the particle, and the detector is located at (x_d, y_d, z_d). The distance from the origin to the detector is r, and the distance from the center of the focal waist to the detector is r'.

In Eqs. (2) $\mathscr{J}_l(kr)$ are Riccati–Bessel functions that are related to spherical Bessel functions $j_l(kr)$ by[11]

$$\mathscr{J}_l(kr) = kr j_l(kr). \qquad (3)$$

The angular functions $\pi_l(\theta)$ and $\tau_l(\theta)$ are related to associated Legendre polynomials by

$$\pi_l(\theta) = \frac{1}{\sin\theta} P_l^1(\cos\theta), \quad \tau_l(\theta) = \frac{d}{d\theta} P_l^1(\cos\theta). \qquad (4)$$

The coefficients g_l are the partial wave amplitudes of the beam, otherwise known as the beam shape coefficients.

The focused laser beam diffractively spreads at values of z beyond the end of its focal waist. In the Fraunhofer zone or far zone of the beam's spreading, the Riccati–Bessel functions become[12]

$$\lim_{kr\to\infty} \mathscr{J}_l(kr) = \sin\left(kr - \frac{l\pi}{2}\right), \qquad (5)$$

and in the near-forward direction (i.e., $\theta \ll 1$), where the beam intensity is expected to be the largest, the angular functions become[13]

$$\begin{aligned}
\lim_{\theta\ll 1} \pi_l(\theta) &= \frac{l(l+1)}{2} [J_0(u) + J_2(u)], \\
\lim_{\theta\ll 1} \tau_l(\theta) &= \frac{l(l+1)}{2} [J_0(u) - J_2(u)], \qquad (6)
\end{aligned}$$

where J_0 and J_2 are Bessel functions and

$$u = (l + 1/2)\theta. \qquad (7)$$

Substituting Eqs. (5) and (6) into Eq. (2) we obtain

$$\begin{aligned}
&\mathbf{E}_{\text{beam}}(r, \theta, \phi) \\
&= -iE_0(\cos\phi \hat{u}_\theta - \sin\phi \hat{u}_\phi) \frac{\exp(ikr)}{kr} \\
&\quad \times \sum_{l=1}^{\infty} (l + 1/2) g_l J_0(u) + iE_0(\cos\phi \hat{u}_\theta + \sin\phi \hat{u}_\phi) \\
&\quad \times \frac{\exp(-ikr)}{kr} \sum_{l=1}^{\infty} (-1)^l (l + 1/2) g_l J_2(u), \\
&\mathbf{B}_{\text{beam}}(r, \theta, \phi) \\
&= \frac{-iE_0}{c} (\sin\phi \hat{u}_\theta + \cos\phi \hat{u}_\phi) \frac{\exp(ikr)}{kr} \\
&\quad \times \sum_{l=1}^{\infty} (l + 1/2) g_l J_0(u) + \frac{iE_0}{c} (\sin\phi \hat{u}_\theta - \cos\phi \hat{u}_\phi) \\
&\quad \times \frac{\exp(-ikr)}{kr} \sum_{l=1}^{\infty} (-1)^l (l + 1/2) g_l J_2(u) \qquad (8)
\end{aligned}$$

as the partial wave expansion of the beam fields in the near-forward direction in the far zone.

Physically, one would expect that for $\theta \approx 0°$ the outgoing spherical wave portion of Eqs. (8) would be orders of magnitude larger than the incoming spherical wave portion. This is in fact the case, mathematically, since the $(-1)^l$ factors in Eqs. (8) cause the slowly varying contributions of successive partial waves nearly to cancel for the incoming wave terms. Similarly for $\theta \approx 180°$, when the backscattering version of Eqs. (6) is substituted into Eqs. (2), the incoming spherical wave contribution dominates, which is again what one would expect physically. For outgoing spherical wave dominance at $\theta \approx 0°$, Eqs. (8) reduce to

$$\mathbf{E}_{\text{beam}}(r, \theta, \phi) \approx -iE_0\hat{u}_x \frac{\exp(ikr)}{kr} \sum_{l=1}^{\infty} (l + 1/2) g_l J_0(u),$$

$$\mathbf{B}_{\text{beam}}(r, \theta, \phi) \approx \frac{iE_0}{c} \hat{u}_y \frac{\exp(ikr)}{kr} \sum_{l=1}^{\infty} (l + 1/2) g_l J_0(u). \tag{9}$$

When the incident on-axis beam interacts with the spherical particle, scattered waves are created. The far-zone scattered electric and magnetic fields produced by the interaction are

$$\lim_{r\to\infty} \mathbf{E}_{\text{scattered}}(r, \theta, \phi) = \frac{-iE_0}{kr} \exp(ikr)[-S_2(\theta)\cos\phi\hat{u}_\theta + S_1(\theta)\sin\phi\hat{u}_\phi],$$

$$\lim_{r\to\infty} \mathbf{B}_{\text{scattered}}(r, \theta, \phi) = \frac{-iE_0}{ckr} \exp(ikr)[-S_1(\theta)\sin\phi\hat{u}_\theta - S_2(\theta)\cos\phi\hat{u}_\phi]. \tag{10}$$

In Eqs. (10) the on-axis scattering amplitudes $S_1(\theta)$ and $S_2(\theta)$ are given by

$$S_1(\theta) = \sum_{l=1}^{\infty} \frac{(2l + 1)}{l(l + 1)} g_l[a_l\pi_l(\theta) + b_l\tau_l(\theta)],$$

$$S_2(\theta) = \sum_{l=1}^{\infty} \frac{(2l + 1)}{l(l + 1)} g_l[a_l\tau_l(\theta) + b_l\pi_l(\theta)], \tag{11}$$

and the coefficients a_l and b_l are the partial wave scattering amplitudes of the plane wave Lorenz–Mie theory.[14]

In experiments, the total exterior fields

$$\mathbf{E}_{\text{total}} = \mathbf{E}_{\text{beam}} + \mathbf{E}_{\text{scattered}}, \quad \mathbf{B}_{\text{total}} = \mathbf{B}_{\text{beam}} + \mathbf{B}_{\text{scattered}} \tag{12}$$

are observed rather than the scattered fields alone. This fact is especially important in the near-forward direction where the spreading beam fields and the scattered fields overlap appreciably.

3. Model for the Beam Shape Coefficients

The mathematically precise way of calculating the beam shape coefficients of a known electromagnetic wave is as follows. Consider an on-axis beam with an arbitrary profile that is written in spherical coordinates with respect to the origin of coordinates at the particle center. The radial component of the field vectors has the form[8]

$$E_{\text{beam}}^{\text{radial}} = E_0 \exp(ikr\cos\theta) f(kr, \theta)\sin\theta\cos\phi,$$

$$B_{\text{beam}}^{\text{radial}} = \frac{E_0}{c} \exp(ikr\cos\theta) f(kr, \theta)\sin\theta\sin\phi, \tag{13}$$

where both the beam amplitude profile and the shape of the surfaces of constant phase are contained in the function $f(kr, \theta)$. Assuming that this function is known, the beam shape coefficients g_l are given by[8]

$$g_l = \frac{(-i)^{l-1}}{2} \frac{kr}{j_l(kr)} \frac{1}{l(l + 1)} \int_0^{\pi} \sin^2\theta \, d\theta f(kr, \theta) \times \exp(ikr\cos\theta) P_l^1(\cos\theta). \tag{14}$$

Since the electric and magnetic fields of Eqs. (13) are assumed to be an exact solution of Maxwell's equations, the r dependence in Eq. (14) cancels and the g_l are constants. Unfortunately, the only case of interest for which $f(kr, \theta)$ is exactly known is that of a plane wave for which $f(kr, \theta) = 1$.

As an alternative to the mathematically precise approach, we consider the following approximate method. Experimentally, one can use a detector array to record only the magnitude squared of the beam fields leaving the phase undetermined. Thus in order to calculate the beam shape coefficients, the beam phase must be either separately measured or modeled. We propose modeling it in the following way. Consider the center of the spherical particle to be at the origin of coordinates. Let the center of the beam's focal waist be at the coordinate $(0, 0, z_0)$ with respect to the particle, and let the detector be at the coordinate (x_d, y_d, z_d) in the far zone of the beam as is shown in Fig. 1. Although each individual partial wave of the beam in approximations (9) is an outgoing spherical wave centered on the particle, in the far zone the beam taken as a whole appears to emanate from an effective point source located at the beam waist center, and its electric field is

$$\mathbf{E}_{\text{beam}} = -iE_0\hat{u}_x \frac{\exp(ikr')}{kr'} M(\theta'). \tag{15}$$

In Eq. (15) $\mathbf{r}'$ is the vector from the center of the focal waist to the detector at (x_d, y_d, z_d), θ' is the angle that the vector $\mathbf{r}'$ makes with the z axis, and $M(\theta')$ is the angular dependence of the amplitude profile of the beam in the far zone.

We wish to convert Eq. (15) from the spherical coordinates r', θ' centered on the beam focal waist to the spherical coordinates r, θ centered on the particle in order to make contact with the partial wave

expansion of the beam of approximations (9). This can be accomplished in the following way. For $z_d \gg z_0$ and in the near-forward direction with $x_d \ll z_d$ and $y_d \ll z_d$, we have

$$
\begin{aligned}
r &\approx z_d + \frac{(x_d{}^2 + y_d{}^2)}{2z_d}, \\
\theta &\approx \frac{(x_d{}^2 + y_d{}^2)^{1/2}}{z_d}, \\
r' &\approx z_d - z_0 + \frac{(x_d{}^2 + y_d{}^2)}{2(z_d - z_0)} \approx z_d - z_0 \\
&\quad + \frac{(x_d{}^2 + y_d{}^2)}{2z_d} + \frac{(x_d{}^2 + y_d{}^2)}{2z_d{}^2} z_0, \\
\theta' &\approx \frac{(x_d{}^2 + y_d{}^2)^{1/2}}{z_d - z_0} \approx \frac{\theta}{\left(1 - \frac{z_0}{z_d}\right)}.
\end{aligned} \tag{16}
$$

Using these changes of variable, Eq. (15) becomes

$$
\mathbf{E}_{\text{beam}} \approx -iE_0\hat{u}_x \frac{\exp(ikr)}{kr} M(\theta')\exp(-ikz_0)\exp(ikz_0\theta^2/2). \tag{17}
$$

Finally, comparing approximations (9) and (17) we obtain

$$
\begin{aligned}
&\exp(-ikz_0)\exp(ikz_0\theta^2/2)M(\theta') \\
&\qquad \approx \sum_{l=1}^{\infty} (l + 1/2)g_l J_0[(l + 1/2)\theta]
\end{aligned} \tag{18}
$$

or

$$
\begin{aligned}
&\frac{(2\mu_0 c)^{1/2}kr}{E_0} I_{\text{beam}}(\theta)^{1/2}\exp(-ikz_0)\exp(ikz_0\theta^2/2) \\
&\qquad \approx \sum_{l=1}^{\infty} (l + 1/2)g_l J_0[(l + 1/2)\theta],
\end{aligned} \tag{19}
$$

where from approximation (17) we used

$$
I_{\text{beam}}(\theta) = \frac{E_0{}^2}{2\mu_0 c k^2 r^2} M^2(\theta'). \tag{20}
$$

At this point we assume that a large number of partial waves are required to reconstruct the focused laser beam. As a result we can approximately convert the sum over partial waves into an integral[13] and replace the beam shape coefficients g_l by the continuous function $g(l)$. We then have

$$
\begin{aligned}
&\frac{(2\mu_0 c)^{1/2}kr}{E_0} \exp(-ikz_0) I_{\text{beam}}(\theta)^{1/2} \exp(ikz_0\theta^2/2) \\
&\qquad \approx \int_0^{\infty} l\,\mathrm{d}l\, g(l) J_0(l\theta).
\end{aligned} \tag{21}
$$

Equation (21) can be recognized as a zero-order Hankel transform.[15] Its inverse Hankel transform is

$$
\begin{aligned}
g(l) &\approx \frac{(2\mu_0 c)^{1/2}kr}{E_0} \exp(-ikz_0) \int_0^{\infty} \theta\,\mathrm{d}\theta I_{\text{beam}}(\theta)^{1/2} \\
&\quad \times \exp(ikz_0\theta^2/2) J_0(l\theta).
\end{aligned} \tag{22}
$$

Approximation (22) for integer l is our approximation to the beam shape coefficients for the focused laser beam with the experimental far-zone beam profile $I_{\text{beam}}(\theta)$, which is the central result of this study.

As a test of the accuracy of approximation (22), we consider a Davis first-order Gaussian beam with electric field

$$
\mathbf{E}_{\text{Davis}}(x, y, z = z_0) = E_0 \exp[-(x^2 + y^2)/w_0{}^2]\hat{u}_x \tag{23}
$$

in the beam focal plane.[16] In the far-zone of the beam, the electric field becomes

$$
\begin{aligned}
&\lim_{kr' \to \infty} \mathbf{E}_{\text{Davis}}(r', \theta', \phi') \\
&\qquad = \frac{-iE_0}{kr'} \frac{k^2 w_0{}^2}{2} \exp(ikr')\exp\left(\frac{-k^2 w_0{}^2 \theta'^2}{4}\right)\hat{u}_x.
\end{aligned} \tag{24}
$$

Using the change of variables from r', θ' to r, θ and taking $z_0/z_d \approx 0$, we obtain

$$
I_{\text{Davis}}(\theta) \approx \frac{E_0{}^2}{2\mu_0 c} \frac{1}{k^2 r^2} \frac{k^4 w_0{}^4}{4} \exp\left(\frac{-k^2 w_0{}^2 \theta^2}{2}\right). \tag{25}
$$

Substituting approximation (25) into approximation (22) and performing the Hankel transform of the Gaussian function, we obtain

$$
\begin{aligned}
g_{\text{Davis}}(l) &= \frac{1}{1 - 2iz_0/kw_0{}^2} \exp(-ikz_0) \\
&\quad \times \exp\left(\frac{-l^2/k^2 w_0{}^2}{1 - 2iz_0/kw_0{}^2}\right).
\end{aligned} \tag{26}
$$

Equation (26) is identical to the localized beam shape coefficients for a Davis first-order beam except for the replacement of $l + 1/2$ in Eq. (50) of Ref. 8 by l in Eq. (26). The difference between l and $l + 1/2$ is minor for the experiment described in Section 4 since approximately 340 partial waves are involved in the scattering.

4. Experimental Verification

The experimental procedure is described in detail in Ref. 6. Briefly, a spatially unfiltered Ar^+ laser operated in the TEM_{00} mode of the $\lambda = 0.5145$ μm line was focused using a 100-mm focal-length lens. At a distance of 146 ± 1.5 mm beyond the beam's focal waist, the beam intensity was measured using a 505-element CCD array interfaced to an 8-bit

frame grabber board. At this distance, the CCD array was in the far zone of the beam (i.e., $2z'/kw_0^2 = 73.8 \gg 1$). The beam intensity after the CCD read noise was subtracted is shown in Fig. 2. Although the experimental beam profile has the same general shape as a Gaussian, there are noticeable differences between Fig. 2 and a pure Gaussian function. These differences were commented on in Ref. 6. Specifically, if the peak intensity of the beam at the detector plane is I_0, the central portion of the beam ($0.25 < I/I_0 < 1.0$) is fit well by a Gaussian function with an electric field half-width of $w_0 = 24$ μm and the outer portions of the beam ($0.01 < I/I_0 < 0.1$) are fit well by another Gaussian function having $w_0 = 18$ μm.

After the far-zone beam profile was measured, a single spherical droplet of dioctyl phthalate (DOP) was levitated using an electrodynamic balance and was positioned at three different locations on the beam axis downstream from the focal waist as in Fig. 1. The spacing between these locations was approximately 12.5 mm. The dioctyl phthalate droplet had radius $a = 25.6 \pm 0.05$ μm and refractive index $n = 1.4845$. Again, for each of the three particle locations, the beam-plus-scattered intensity was measured in the near-forward direction (i.e., $|\theta| \lesssim 1.0°$) and was normalized with respect to the peak beam intensity at the detector. The experimental scattering data are shown in Figs. 3(a)–3(c). In Ref. 6 the positions of the particle with respect to the beam waist were determined by fitting Figs. 3(a)–3(c) with the central region/outer regions two-Gaussian model employed by Hodges *et al.* Based on their fitting procedure, they determined that Figs. 3(a)–3(c) correspond to $z_0 = -5.0$ mm, $z_0 = -18.2$ mm, and $z_0 = -30.0$ mm, respectively. The coordinate of the beam focal waist, z_0, is negative since the beam focuses before the origin of coordinates.

Before employing our beam shape coefficient model of approximation (22) to fit the experimental scattering data, the beam profile data of Fig. 2 was preprocessed in the following way. First, with the center of the beam normalized to unit intensity, the beam

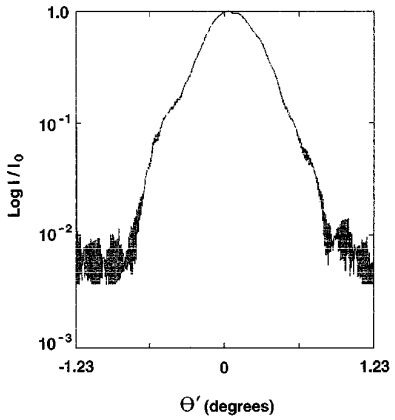

Fig. 2. Intensity as a function of angle for a focused Ar^+ laser beam at a distance of $z_d = 146 \pm 1.5$ mm beyond the beam focal waist. The detector is in the far zone of the beam.

was thresholded at $I_{\text{beam}} = 0.01$ since the quantization error of the intensity digitization was $I_{\text{quantization}} \approx 0.004$. Since an on-axis beam is defined to be symmetric about the beam axis, the best-fit beam axis was found for $0.01 \leq I_{\text{beam}} \leq 1.0$, and the beam intensities at equal distances to either side of the axis were averaged. The experimental scattering data of Figs. 3(a)–3(c) were not symmetrized in this way. As mentioned previously, it was found in Ref. 6 that the outer portion of the beam (i.e., $0.01 \lesssim I_{\text{beam}} \lesssim 0.1$) is fit well by a Gaussian profile of beam waist radius $w_0 = 18$ μm. Our thresholded and symmetrized beam profile was continued from $I_{\text{beam}} = 0.01$ to $I_{\text{beam}} = 10^{-8}$ using the $w_0 = 18$ μm Gaussian model.

This continuation was made in order to eliminate artifacts that were found to occur in the computed values of g_l caused by the experimental cutoff of the θ integral in approximation (22). The elimination of the artifacts in the g_l was tested by reconstructing the beam profile using approximation (18) after calculating the g_l using approximation (22). Testing this reconstruction procedure first on the truncated Gaussian beam profile

$$I_{\text{Gaussian}}(\theta) = \exp(-\theta^2/4s^2) \text{ for } 0 \leq \theta \leq \theta_{\max} \quad (27)$$

with

$$s = \frac{1}{kw_0}, \quad (28)$$

the reconstructed beam was found to reproduce the Gaussian function of Eq. (27) for $0 \leq \theta \lesssim \theta_{\max}$ virtually exactly when the largest partial wave $l_{\max}$ satisfied

$$l_{\max} \gtrsim 4/s. \quad (29)$$

Regardless of the value of $\theta_{\max}$, the reconstructed beam was always found to oscillate about the Gaussian profile of Eq. (27) for $\theta \approx \theta_{\max}$. Extending our thresholded and averaged beam to $I_{\text{beam}} = 10^{-8}$ thus ensured that any artifact in the g_l that is due to the cutoff of the θ integral at $\theta_{\max}$ would be moved out of the intensity region of interest so as to affect only beam intensities that are orders of magnitude below the intensity cutoff of the scattering data at $I/I_0 = 0.01$ in Figs. 3(a)–3(c).

Next, this reconstruction procedure was tested on the thresholded and symmetrized experimental beam derived from Fig. 2. Approximation (22) was evaluated for $l_{\max} = 1500$ for a number of values of the beam waist particle spacing z_0. This value of $l_{\max}$ is a factor of 2 above the beam reconstruction stability requirement of inequality (29) (i.e., $w_0 = 18$ μm gives $s = 0.00455$ and $l_{\max} \gtrsim 879$). In addition, if the detector grid is too coarse and l is too large, the evaluation of approximation (22) by numerical integration becomes imprecise because $l\Delta\theta$ is comparable to or larger than the periodicity of Bessel function J_0. For our 505-element detector array

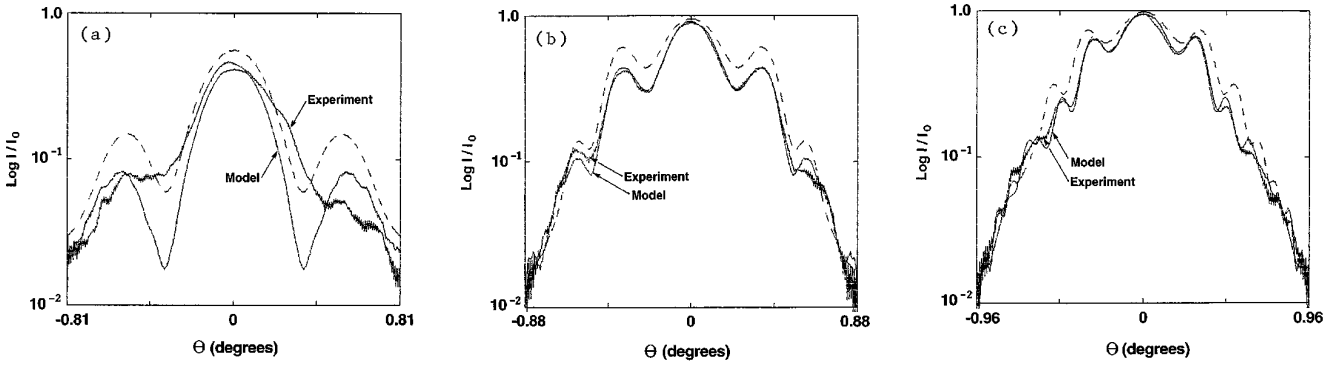

Fig. 3. Beam-plus-scattered intensity as a function of scattering angle θ for a beam waist particle spacing of (a) $z_0 = -4.0$ mm, (b) $z_0 = -14.5$ mm, (c) $z_0 = -25.0$ mm. The experimental data are from Figs. 10(b), 10(d), and 10(f) of Ref. 6, respectively, and the theoretical intensity is from Eqs. (10)–(13) and (20) and approximation (22). The single-Gaussian fit to the data for $w_0 = 18$ μm from Ref. 6 is given by the dashed curves.

with $\Delta\theta = 4.9 \times 10^{-3}$ deg, the Nyquist partial wave for $J_0(l\theta)$ is $l_{\text{Nyquist}} = 18{,}350$. Our choice of $l_{\max} = 1500$ is a factor of 12 below the Nyquist limit thus ensuring the accuracy of numerical integration. Again after the g_l were computed, the symmetrized beam was reconstructed using approximation (18). As before, the beam reconstruction virtually exactly reproduced the original beam for $I_{\text{beam}} > 10^{-7}$.

Now being confident that the beam shape coefficients were being computed accurately, the scattered electric field was computed using Eqs. (10) and (11) and the beam electric field was evaluated using the left-hand side of approximation (21) along with the experimentally measured profile. The two fields were added as in Eqs. (12), and the resulting beam-plus-scattered intensity was determined. The only adjustable parameter in our model is the distance z_0 between the beam waist center and the particle. This distance was varied to fit the angular positions of the subsidiary maxima of the experimental data. There is no intensity scaling factor in our model. The resulting beam-plus-scattered intensity is shown in Figs. 3(a)–3(c) for $z_0 = -4.0$ mm, $z_0 = -14.5$ mm, and $z_0 = -25.0$ mm, respectively. In Figs. 3(b) and 3(c) the angular width of the central maximum and the positions of the subsidiary maxima are fit well with our model. Further the entire intensity profile is fit well in contrast to Ref. 6 in which a Gaussian function of $w_0 = 24$ μm for the beam fits only the small-angle (i.e., $0.25 \lesssim I/I_0 \lesssim 1.0$) data and another Gaussian function of $w_0 = 18$ μm for the beam fit only the large-angle (i.e., $0.01 \lesssim I/I_0 \lesssim 0.1$) portions of the experimental intensity profile. The outer $w_0 = 18$ μm Gaussian beam fit to the experimental data from Ref. 6 is also shown in Figs. 3(a)–3(c) for comparison. The interference structure in Figs. 3(a)–3(c) is due to the fact that the surfaces of constant phase of the incident beam and the scattered wave have different radii of curvature at the detector plane. As one scans along the detector plane, the two waves of different curvature alternately constructively and destructively interfere according to the $\exp(ikz_0\theta^2/2)$ factor in approximation (17).

For all three sets of data the experimental fringe contrast for the outer portions of the data is often lower than our theoretical predictions. This appears not to be due to the finite pixel size since each relative minimum extends over at least 8 pixels. Small differences between the left-hand and right-hand sides of the unsymmetrized experimental data in Figs. 3(a)–3(c) mirror both the slight asymmetry of the original beam in Fig. 2 and the fact that the particle may have been slightly off axis with respect to the beam. Also, since it is experimentally impossible to measure the distance z_0 to an accuracy that is substantially smaller than a wavelength over a distance of many millimeters, the phase of the $\exp(-ikz_0)$ factor in approximations (19)–(22) is undetermined. When one constructs the beam-plus-scattered intensity, this $\exp(-ikz_0)$ factor is of no consequence, however, since it appears in an identical way in both the scattered field using Eqs. (10) and (11) and approximation (22) and in the beam field using the left-hand side of approximation (21).

In Fig. 3(a) the predictions of the single-Gaussian model with $w_0 = 18$ μm and $z_0 = -5.0$ mm of Ref. 6 and the predictions of our model with $z_0 = -4.0$ mm are similar. (For our model with $z_0 = -5.0$ mm they are almost identical.) But neither fits the experimental data well. Both models reasonably fit the shape of the central peak and the rate of fall off of the outer portions of the experimental data but grossly overestimate the interference structure. Perhaps this overestimation is not surprising for two reasons. First, for a Gaussian beam with $w_0 = 18$ μm, the point of maximum wave-front curvature occurs at $z_0 = \pm 2.0$ mm, whereas for $w_0 = 24$ μm, it occurs at $z_0 = \pm 3.5$ mm. Since the data of Fig. 3(a) was obtained only slightly beyond the point of maximum wave-front curvature, small inaccuracies in modeling the phase of the beam in this region may well produce large errors in the structure of the scattered wave/incident beam interference described above. Second, for a particle of radius 25.6 μm the first far-zone diffraction zero occurs at $\theta = 0.70°$. At this angle the phase of the diffracted field shifts by 180°,

which also adds to the complexity of the scattered wave/incident beam interference there.

Figure 11 of Ref. 6 shows the experimental scattered intensity for $8° \leq \theta \leq 15°$ along with the predictions of the two-Gaussian beam model of Hodges *et al.* Both the central and outer Gaussian models fit the laboratory data well. The reason for this is twofold. First, this angular interval is beyond the spreading width of the incident beam so no incident beam/scattered field interference occurs. Second, for $z_0 = -4.0$, -14.5, and -25.0 mm, the effective beam half-width at the location of the particle is approximately 41, 133, and 237 μm, respectively. The rays reflected by the particle in this angular interval strike it approximately 25.5-μm off-axis, whereas the rays transmitted through the particle in this angular interval strike it approximately 7.5-μm off-axis. In all cases these off-axis positions are near the center of the local beam profile (i.e., the beam intensity is $I_{\text{beam}} \gtrsim 0.46$) where the beam is well described by a Gaussian of width $w_0 = 24$ μm. The deviations from an ideal Gaussian profile that occur at lower beam intensities (i.e., $I_{\text{beam}} \lesssim 0.25$) are not observed in scattering from a particle of this size placed this far downstream from the beam waist when the scattering angle is larger than approximately 2°. Thus we did not examine the predictions of our beam shape coefficient model of approximation (22) for the angular interval of Fig. 11 of Ref. 6. This points up an important issue concerning our model for scattering by a non-Gaussian beam. The deviations between the beam of Fig. 2 and an exact Gaussian are significant but not overwhelming. As a result, the differences between Gaussian beam scattering theory and non-Gaussian beam scattering theory are most apparent in the angular region where the incident beam superposes with the scattered wave. This occurs in the near-forward direction, which is what we have analyzed in this experiment.

A number of previous experiments have also been used to examine near-forward scattering of a focused laser beam in which the spreading beam field and the scattered field overlap appreciably.[17–19] Figure 2 of Ref. 17 shows both experimental data and the results of diffraction theory for $a = 22$ μm, the beam half-width at the position of the particle $w(z_0) = 43$ μm, and $0° \leq \theta \lesssim 0.92°$. The comparison between theory and experiment is excellent for $10^{-3} \lesssim I/I_0 \leq 1.0$, indicating that the expanded and spatially filtered beam of Ref. 17 was almost exactly Gaussian in shape. Figure 12 of Ref. 18 shows both experimental data and the results of Gaussian beam scattering theory for $a = 34.8$ μm, $w(z_0) = 42.6$ μm, and $0° \leq \theta \lesssim 1.72°$. The deviation of Gaussian beam scattering theory from the data for $\theta \gtrsim 0.6°$ indicates that the spatially unfiltered beam of Ref. 18 deviates from a Gaussian for $I/I_0 \lesssim 10^{-2}$. Figures 8–16 of Ref. 19 are concerned with an off-axis beam. But again there are small deviations between Gaussian beam theory and experiment for $I/I_0 \approx 10^{-2}$ that the authors tentatively attributed to "imperfections in the Gaussian character of the beam . . . because of the finiteness of the laser source." Based on these results, it would be interesting to test to what degree spatial filtering would eliminate the deviations of an unfiltered beam, such as we have in Fig. 2, from an ideal Gaussian shape. The price one pays for spatial filtering, however, is a greatly reduced beam intensity. This intensity reduction was the reason that we did not spatially filter the laser beam in this experiment.

Over the last few years a number of papers have been published claiming to extend Lorenz–Mie scattering theory from plane wave incidence to arbitrary beam incidence.[3–5] From a theoretical point of view, these claims were correct. But from an experimental point of view they did not answer the question of how to obtain the beam shape coefficients of an actual laboratory beam. The good agreement between our beam shape coefficient model and the experimental results of Figs. 3(b) and 3(c) provides a tentative answer to this question for an axisymmetric on-axis beam if one measures its far-zone intensity profile. Our phase modeling procedure has not been tested on severely non-Gaussian axisymmetric beams or on nonaxisymmetric on-axis beams. In the first of these cases it is our belief that our model will work satisfactorily if the surfaces of constant phase of the beam are not too contorted. For the second of these cases the partial wave expansion of the beam depends on the partial wave modes l and m, where $1 \leq l < \infty$ and $-l \leq m \leq l$ and is thus outside the scope of this paper. The beam shape coefficients of an axisymmetric off-axis beam also depend on l and m and will be the subject of a separate publication.

We thank Gérard Gouesbet of l'Institut National des Sciences Appliquées de Rouen, France, for bringing the problem of obtaining the beam shape coefficients of an actual laser beam to our attention.

References

1. E. E. M. Khaled, S. C. Hill, P. W. Barber, and D. Q. Chowdhury, "Near-resonance excitation of dielectric spheres with plane waves and off-axis Gaussian beams," Appl. Opt. **31,** 1166–1169 (1992).
2. E. E. Khaled, S. C. Hill, and P. W. Barber, "Scattered and internal intensity of a sphere illuminated with a Gaussian beam," IEEE Trans. Antennas Propag. **41,** 295–303 (1993).
3. G. Gouesbet and G. Gréhan, "Sur la généralisation de la théorie de Lorenz-Mie," J. Opt. (Paris) **13,** 97–103 (1982).
4. G. Gouesbet, B. Maheu, and G. Gréhan, "Light scattering from a sphere arbitrarily located in a Gaussian beam, using a Bromwich formalism," J. Opt. Soc. Am. A **5,** 1427–1443 (1988).
5. J. P. Barton, D. R. Alexander, and S. A. Schaub, "Internal and near-surface electromagnetic fields for a spherical particle irradiated by a focused laser beam," J. Appl. Phys. **64,** 1632–1639 (1988).
6. J. T. Hodges, C. Presser, G. Gréhan, and G. Gouesbet, "Forward scattering of a Gaussian beam by a nonabsorbing sphere," Appl. Opt. **34,** 2120–2132 (1995).
7. G. Gréhan, B. Maheu, and G. Gouesbet, "Scattering of laser

beams by Mie scatter centers: numerical results using a localized approximation," Appl. Opt. **25,** 3539–3548 (1986).
8. J. A. Lock, "Contribution of high-order rainbows to the scattering of a Gaussian laser beam by a spherical particle," J. Opt. Soc. Am. A **10,** 693–706 (1993).
9. J. R. Reitz, F. J. Milford, and R. W. Christy, *Foundations of Electromagnetic Theory,* 3rd ed. (Addison-Wesley, Reading, Mass., 1979), Section 17.5.
10. G. Gouesbet, B. Maheu, and G. Gréhan, "The order of approximation in a theory of the scattering of a Gaussian beam by a Mie scatter center," J. Opt. (Paris) **16,** 239–247 (1985).
11. M. Abramowitz and I. A. Stegun, eds., *Handbook of Mathematical Functions* (Dover, New York, 1964), Section 10.3.
12. G. Arfken, *Mathematical Methods for Physicists* (Academic, New York, 1985), Eq. (11.158).
13. H. C. van de Hulst, *Light Scattering by Small Particles* (Dover, New York, 1981), Section 12.32.
14. Ref. 13, Section 9.22.
15. Ref. 12, Section 15.1.
16. L. W. Davis, "Theory of electromagnetic beams," Phys. Rev. A **19,** 1177–1179 (1979).
17. J.-P. Chevaillier, J. Fabre, and P. Hamelin, "Forward scattered light intensities by a sphere located anywhere in a Gaussian beam," Appl. Opt. **25,** 1222–1225 (1986).
18. J. P. Chevaillier, J. Fabre, G. Gréhan, and G. Gouesbet, "Comparison of diffraction theory and generalized Lorenz-Mie theory for a sphere located on the axis of a laser beam," Appl. Opt. **29,** 1293–1298 (1990).
19. F. Guilloteau, G. Gréhan, and G. Gouesbet, "Optical levitation experiments to assess the validity of the generalized Lorenz–Mie theory," Appl. Opt. **31,** 2942–2951 (1992).